

Thermal conductivity of ^4He I near T_λ from vapor pressure to 28 bars: Comparison of experiment and theory

W. Y. Tam and Guenter Ahlers

Department of Physics, University of California, Santa Barbara, California 93106

(Received 19 August 1985)

We compare recent thermal-conductivity measurements near the superfluid transition temperature $T_\lambda(P)$ with recent complete two-loop-order field-theoretical calculations of the renormalization-group recursion relations and of the relation between the conductivity and the dynamic variables of the theory. The comparison involves a numerical integration of the recursion relations, and thus contains certain dynamic transients to all orders. We find excellent agreement over a wide range of pressure and reduced temperature when the complete two-loop theory is used. Neglect of any of a number of ingredients of the theory results in a deterioration of the agreement with experiment. In particular, it is necessary to use the full asymmetric planar spin model (model F) of the dynamics, and to include singular static transients in the theory, in order to obtain a good fit. From our analysis above $T_\lambda(P)$, and a calculation of the second-sound damping D_2 below $T_\lambda(P)$ based on the symmetric planar spin model (model E), we estimate D_2 . As in earlier work, we still find small differences between theory and experiment, and attribute them to the use of model E in the derivation of the formula for D_2 .

I. INTRODUCTION

Two major advances towards the elucidation of the dynamics of the superfluid transition have occurred recently. On one hand, the relationship between the thermal conductivity λ and the variables of the renormalization-group model¹ for the dynamics of the superfluid transition (the asymmetric planar spin model, model F) have been obtained²⁻⁴ from perturbation theory to second order in the coupling constants. On the other, a new set of measurements of $\lambda(P, t)$ (t is the reduced temperature [Eq. (1) below] and P the pressure) has been made⁵ which is considerably more accurate and covers a wider range of P and t than previous experimental results. For these two reasons we are now in a position to perform a quantitative test of the theory by a detailed comparison with experiment, at least in the temperature region $t \gtrsim 10^{-3}$ or 10^{-4} , where there exists a weak-coupling regime⁶ and where therefore the perturbation calculations should constitute a controlled approximation to the full model of the dynamics. In this paper, we largely follow the procedures developed earlier,⁶⁻⁸ and present the results of such a comparison. They indicate that there is agreement between experiment and theory at a highly quantitative level over the entire experimentally accessible range of P and t .⁹

The Langevin equations of Halperin, Hohenberg, and Siggia,¹ which are known as model F [Eqs. (2.1) of Ref. 1 or Eqs. (2.3)–(2.6) of Ref. 4], are expected to contain the full contributions from thermal diffusion and second sound to the dynamics of the superfluid transition. Although these equations ideally should provide the starting point for the calculation of the relationship between the

physically measurable quantities [such as $\lambda(t)$ or its effective amplitude $\hat{R}_\lambda(t)$] and the parameters of the model, such a calculation to sufficiently high order in perturbation theory is difficult. Therefore Halperin *et al.* proposed that the simpler symmetric planar spin model, known as model E, which neglects the coupling between the specific heat C_P and the dynamic variables, might still be useful for a semiquantitative description of the dynamics of liquid helium. Their suggestion was based on the fact that the specific-heat exponent α is negative for the superfluid transition,^{10,11} i.e., that C_P goes to a constant as $T \rightarrow T_\lambda$. Indeed, sufficiently close to T_λ models E and F (with $\alpha < 0$) will give the same dynamics, but since $|\alpha| \ll 1$ ($\alpha = -0.016 \pm 0.003$),¹¹ the close agreement between the two models breaks down for unrealistically small values of $|t|$ and the singularity of the specific heat leads to very slow transients which are important in any experimentally accessible range of t . Halperin *et al.* attempted to partly compensate for these static transients by including the full singular (albeit finite) specific heat in the relationship between λ and its effective amplitude $\hat{R}_\lambda(t)$ [see Eq. (2) below], but neglecting its coupling to the dynamic variables f and ω in the renormalization-group flow equations. This approximation, now known as model E_s,⁶ was used by Dohm and Folk⁷ in their early analysis of the thermal conductivity. Although model E_s gives a fairly accurate description of the dynamics at small t (say, $t \leq 10^{-5}$), it actually provides a worse fit to the data than model E for larger t (see Fig. 8 of Ref. 6). Therefore the full model F is required to give an accurate description of the dynamics over a wide experimentally accessible range of the reduced temperature. Because of the difficulties involved in obtaining a complete perturba-

tion calculation to second order in the coupling constants f , w , γ , and u , Ahlers *et al.*⁶ used a version of model F in which the one-loop terms in the flow equations were based on model F, but the two-loop terms were calculated only approximately from model E. This version provided a good fit to the data when an empirical three-loop term with an adjustable coefficient was added to the flow equations. Soon thereafter Dohm and Folk¹² published an analysis of the experimental data, using new (as yet unpublished) complete two-loop flow equations² based entirely upon model F. However, both this analysis¹² and the one by Ahlers *et al.*⁶ retained the one-loop result for the relationship between \hat{R}_λ and the dynamic variables. Furthermore, both of these two approximations neglected the (transient) singular temperature dependence of the static four-point coupling constant $u(t)$. These last deficiencies in the theory have finally been removed by Dohm.²⁻⁴ He obtained both the flow equations² and the relation⁴ $\hat{R}_\lambda(f, w, u, \gamma)$ to two-loop order completely from model F. In addition, he calculated approximate relationships for static properties³ which make it possible to estimate quite well the t dependence of the static coupling constants $u(t)$ and $\gamma(t)$ from the experimentally determined^{10,11} specific heat. Thus, we now have a complete two-loop model-F theory which takes static transients into account to good accuracy.

Traditionally, theoretical predictions of properties near critical points were expanded in the form of power laws, and these expansions were compared with experimental results. For static properties it became clear over a decade ago¹⁰ that, in general, at least one confluent singular term, corresponding to singular transients in the theory, had to be included in the expansion in order to achieve quantitative agreement with experiment. A similar approach to the dynamics of superfluid helium, using a single confluent singularity, met only with semiquantitative success^{9,13} because in this case the transients are *extremely* slow. They would be taken into account adequately only by including an unrealistically large number of confluent singular terms. Therefore it was suggested by Hohenberg, Halperin, and Nelson,¹³ and independently by Dohm and Folk,⁷ that the power-law expansion of the theory would better be replaced by a numerical integration of the full nonlinear recursion relations of the renormalization-group theory. This approach would automatically include transients to all orders without any increase in the number of adjustable parameters. Such an analysis was indeed carried out by Dohm and Folk,^{7,12} and by Ahlers, Hohenberg, and Kornblit.⁶ In the present work we will follow the general procedures developed by those authors.

In our comparison with the experimental data we will fit the theory to the measurements by adjusting three nonuniversal parameters. These parameters will be the initial values, chosen at some reference temperature t_0 , which are used to integrate the flow equations from t_0 to arbitrary t . Theoretically, they could only be obtained from a truly microscopic theory of liquid helium, and thus at this time they must be taken from experiment. They may depend upon the pressure, and thus may be chosen independently for each isobar. We remark that the conventional power-law analyses of properties near criti-

cal points also involve nonuniversal adjustable parameters (the background and the amplitudes) which play a role similar to the initial values in the procedure used by us. In our analysis there are only three parameters for a given P . Nonetheless, it seems important to us to determine whether the excellent agreement between theory and experiment which we will report below is merely the result of "curve fitting," or whether it genuinely provides evidence in support of the validity of the theory. Thus, we deliberately introduced various approximations into the theory (see Sec. III B). Most of these approximations resulted in a deterioration of the fits to the data even though the fits in some cases involved equally as many adjustable parameters. Therefore we feel that the excellent fit to the data over a wide range of t and along all isobars from vapor pressure to 28 bars, which could be obtained *only* with the complete two-loop model-F flow equations and the inclusion of static transients in $u(t)$, is a significant test of the theory.

It became evident from previous comparisons of experiment and theory, as well as from the present work, that the dynamics of the superfluid transition is very rich.⁶⁻⁸ This richness is reflected in a number of features, including the following.

(i) There exists a weak-coupling regime at large t with a crossover to a critical (strong-coupling) regime at a small but experimentally accessible reduced temperature t_c .

(ii) The value of t_c has a strong pressure dependence, changing from about 10^{-2} at saturated vapor pressure (SVP) to about 10^{-3} at 28 bars.

(iii) Whereas the static properties near T_λ can be described very well for $t \lesssim 10^{-2}$ by a leading singularity and transients in the form of a single confluent power-law term,¹⁰ the dynamics contains extremely slow transients which cannot fruitfully be expanded in power laws.

(iv) Although the specific heat C_P remains finite at T_λ ,^{10,11} its singularity couples nonlinearly to the dynamic variables and, as discussed above, the asymmetric planar spin model (model F) (Ref. 1) which includes this coupling must be used in order to obtain a quantitative fit to the data.

(v) The confluent singularities of the various static properties which enter as parameters into the dynamic equations must be taken into account in order to obtain a quantitative fit of the conductivity. These singularities are known from independent measurements of static properties^{10,11} and have a strong pressure dependence which significantly influences the pressure dependence of the dynamics.

All the above features are correctly reflected in both theory¹⁻⁴ and experimental data.⁵ It is because of this complicated dynamics that we regard the quantitative agreement between measurements and calculation as one of the most spectacular successes of the renormalization-group theory¹⁴ of critical phenomena.

The remainder of this paper is organized as follows. In the next section the data, the theoretical model, and the numerical procedure used in this comparison are discussed. That section is of necessity rather detailed, and some readers may wish to skip it and proceed immediately to Sec. III, where the results of the comparison between

experiment and theory are presented. Since Sec. III is not very long, we felt that a summary was superfluous.

II. DATA, THEORY, AND PROCEDURE

A. Data

The new thermal-conductivity measurements reported in Ref. 5 (to be referred to as I hereafter) were performed in a number of cells with various spacings. We will concentrate our analysis on the most accurate and precise data of I, namely those obtained in "cell F" with a spacing $d=0.203$ cm. In the various fits we will usually use only those points which are quoted explicitly in Table VI of I; but in the figures we will sometimes show more points by including some of the unpublished data which are available in Ref. 15. We will also present some fits based on cell-E data ($d=0.452$ cm), which are quoted in Table V of I.

The theory^{1,16,17} predicts that $\lambda \sim t^{-\nu/2}$, where

$$t = T/T_\lambda(P) - 1 \quad (1)$$

and where ν is the exponent of the correlation length ξ . It is convenient to remove this strong dependence upon t from the experimental data, and to compare the dimensionless effective amplitude [see, e.g., Eq. (4.6) of Ref. 4]

$$\hat{R}_\lambda(t) = (\lambda/k_B)/g_b(\xi C_P/k_B)^{1/2} \quad (2)$$

with the predictions of the theory. As t vanishes, $\hat{R}_\lambda(t)$ is predicted to approach a universal value R_λ . Thus, $\hat{R}_\lambda(t)$ contains only the temperature dependence of the slow transients; but these transients are very slow indeed and R_λ is not directly accessible to experimental measurement. However, the comparison between theory and experiment now becomes very sensitive to fine detail because only the transients are being compared.

In Eq. (2), C_P is the heat capacity at constant pressure per unit volume, and is given by

$$C_P = A[(1/\alpha)(t^{-\alpha} - 1) + \tilde{D}t^{\Delta-\alpha} + \tilde{B}] \quad (3a)$$

with

$$A(T) = A_0(1 + a_1t + a_2t^2), \quad (3b)$$

$$\tilde{B}(T) = \tilde{B}_0(1 + b_1t + b_2t^2), \quad (3c)$$

$$\tilde{D}(T) = \tilde{D}_0(1 + d_1t), \quad (3d)$$

$$\alpha = -0.016, \quad (3e)$$

$$\Delta = 0.50. \quad (3f)$$

The parameters A_0 , \tilde{B}_0 , \tilde{D}_0 , a_i , b_i , d_1 depend upon the pressure, and for the isobars of the thermal-conductivity data they are given in Table XI of I (see also Sec. III C 2 and Appendix E of I for further discussion of C_P). In Eq. (2), k_B is Boltzmann's constant and the bare dynamic coupling constant g_b is given in terms of measurable quantities by^{1,4}

$$g_b = \sigma_\lambda k_B T_\lambda / \hbar. \quad (4)$$

Here $\sigma_\lambda = S_\lambda / R$, where $S_\lambda(P)$ is the entropy per mole at

$T_\lambda(P)$ and R is the gas constant. Values of g_b can be found in Table X of I. The correlation length

$$\xi = \xi_0 t^{-\nu} (1 + D_\xi t^\Delta) \quad (5)$$

in Eq. (2) has been obtained¹¹ from measurements¹⁰ of the superfluid density ρ_s/ρ . Its amplitude $\xi_0(P)$ is given in Table XI of I for the isobars of interest. Its leading exponent is¹¹

$$\nu = 0.672 \quad (6a)$$

and Δ is given by Eq. (3f).

The confluent singularity amplitude is related to that of C_P by^{18,19}

$$D_\xi = 0.102 \tilde{D}_0. \quad (6b)$$

Table XI of I gives $\tilde{D}_0(P)$. This completes the information necessary to obtain $\hat{R}_\lambda(t)$ from $\lambda(t)$. Values of \hat{R}_λ corresponding to the experimental points for λ have been given in I, Table VI.

The lowest-order static transient $D_\xi t^\Delta$ has an exponent $\Delta \cong 0.5$ and therefore can contribute significantly even when t is quite small. Thus it has been included via Eq. (5) in the experimental determination of \hat{R}_λ . We have neglected singular terms of order $t^{2\Delta}$ and $t^{1-\alpha}$, and regular transients of order t , all of which effectively look like contributions of order t to \hat{R}_λ . We expect the neglected contributions to be small only when t is small, and therefore shall restrict the comparison of \hat{R}_λ with the theory to values of t less than 10^{-2} . For large t it is better to make the comparison with a high-temperature expansion of the theory⁶ which involves λ itself rather than \hat{R}_λ .

B. Model

We shall use the complete two-loop field-theoretic calculations by Dohm²⁻⁴ of the relationship between the physically measurable quantities [such as $\hat{R}_\lambda(t)$] and the parameters of the asymmetric planar spin model (model F) of Halperin *et al.*¹ We shall largely follow the notation and sign convention of Dohm.²⁻⁴ His complete theoretical results are quite complicated and need not be reproduced here. We will define only those parameters and variables which must be identified in order to specify precisely the fits of the theory to the data that were performed by us. At the same time we will also identify the necessary experimental input.

The independent variable l of the renormalization-group flow equations is related to physically measurable quantities by

$$e^l = t_0^\nu (1 + D_\xi t_0^\Delta)^{-1} \xi / \xi_0, \quad (7a)$$

where t_0 is an arbitrarily chosen reference reduced temperature (we have always used $t_0 = 10^{-2}$), and where ξ/ξ_0 is given by Eq. (5). The variable l defined by Eq. (7a) differs from that used by Dohm (which we will call l_D). The two are related by

$$l = -\ln l_D + \text{const}. \quad (7b)$$

We prefer the definition Eq. (7a) because $l \sim -\ln t$. The flow equations must be integrated over several decades of t , and uniform steps in l , corresponding to nearly uniform

steps in $\ln t$, are natural in the numerical procedure. The exponents ν and Δ and the amplitude D_ξ are given by Eqs. (6) and (3f). The fixed point of interest of the theory corresponds to $l \rightarrow \infty$, and by Eqs. (5) and (7) this implies $t \rightarrow 0$ (i.e., $\xi \rightarrow \infty$). The scale of l is set by the choice of t_0 , and for $t = t_0$ we have $l = 0$. In our fits we needed to invert Eq. (7a) numerically to obtain $t(l)$.

The effective amplitude $\hat{R}_\lambda[l(t)]$ is given by [see Eq. (4.12) of Ref. 4]

$$\hat{R}_\lambda = [4\pi f w' (1 - 2\gamma^2 - 16\gamma^2 u)]^{-1/2} (1 - f/4 + fM_3). \quad (8)$$

Here w' is the real part of

$$w(l) = w'(l) + iw''(l). \quad (9)$$

Following Dohm,⁴ we introduce

$$F^2 = f(l)w'(l) \quad (10)$$

with $F > 0$. The choice of a positive F will result in $w'' > 0$. The dynamic variables f and w are given by the renormalization-group flow equations²⁰

$$dF/dl = -\beta_F(w, F, u, \gamma) \quad (11a)$$

and

$$dw/dl = -\beta_w(w, F, u, \gamma). \quad (11b)$$

In order to compare experiment with theory, the (complex) differential equations (11) must be integrated numerically. In Eqs. (8) and (11), $u(l)$ is the renormalized four-point static coupling constant of the Ginzburg-Landau-Wilson Hamiltonian, and $\gamma(l)$ is the renormalized coupling constant describing the coupling between the order parameter and the entropy fluctuations [see Eqs. (2.6) of Ref. 4 for a definition of the corresponding bare parameters γ_0 and \tilde{u}_0]. The function $M_3(w, F, \gamma)$ is quite complicated, and is given by Eqs. (4.13)–(4.17) of Ref. 4. It will not be reproduced here. The beta functions needed in Eq. (11), and the related β_f in

$$\begin{aligned} df/dl &= -\beta_f(w, f, u, \gamma) \\ &= -(2F/w')\beta_F + [F^2/(w')^2]\text{Re}(\beta_w) \end{aligned} \quad (12)$$

are also too complicated to repeat here, and have been given by Dohm.²

For $t \leq 10^{-2}$, the static coupling constant $u[l(t)]$ which occurs in Eqs. (8) and (11) was obtained by numerically inverting the relation [see Eq. (6.1) of Ref. 3]

$$\frac{R_0(t) - 1}{\alpha_{\text{eff}}^+(t)} = \frac{[(2u)^{-1} - 2][2 - \xi_r(u)]}{2\{2 - [1 - 2\xi_r(u)](1 + 8u) + 8\beta_u(u)\}}, \quad (13)$$

where $R_0(t)$ and $\alpha_{\text{eff}}^+(t)$ are related to the heat capacity by

$$R_0(t) = C_P^-(|t|/2)/C_P^+(t) \quad (14)$$

and

$$\alpha_{\text{eff}}^+ = -d \ln C_P^+(t)/d \ln t. \quad (15)$$

Here C_P^+ and C_P^- refer to C_P above and below T_λ , respectively, and are given by Eq. (3a). For $t > 0$ the amplitudes A , \tilde{D} , and \tilde{B} are given by Eqs. (3b)–(3d). The exponents α and Δ are the same on the two sides of T_λ . The amplitudes A' , \tilde{B}' , and \tilde{D}' , which with Eq. (3a) give C_P below

T_λ , are universally related to the corresponding quantities above T_λ by¹¹

$$A/A' = 1.068, \quad (16)$$

$$\tilde{D}_0/\tilde{D}'_0 = 1.03, \quad (17)$$

and

$$A(\tilde{B} - 1/\alpha) = A'(\tilde{B}' - 1/\alpha). \quad (18)$$

The last equation follows because, for $\alpha < 0$, C_P is continuous at T_λ .

The function $\xi_r(u)$ in Eq. (13) is well approximated by Eq. (6.6) of Ref. 3, i.e.,

$$\xi_r(u) = \tilde{\xi}_r(u) + [2 - \nu^{-1} - \tilde{\xi}_r(u^*)](u/u^*)^3, \quad (19)$$

where

$$\tilde{\xi}_r(u) = 16u - 160u^2. \quad (20)$$

In Eq. (19), u^* is the fixed-point value of u to be given by Eq. (25) below. Equation (19) gives $\xi_r(u^*) = 2 - \nu^{-1}$. With Eq. (6a) we have

$$\xi_r(u^*) = 0.5119. \quad (21)$$

The beta function $\beta_u(u)$ is well approximated by Eq. (6.7) of Ref. 3, i.e.,

$$u^{-1}\beta_u(u) = u^{-1}\tilde{\beta}_u(u) - (u^*)^{-1}\tilde{\beta}_u(u^*)(u/u^*)^3, \quad (22)$$

with

$$u^{-1}\tilde{\beta}_u(u) = -1 + 40u - 960u^2. \quad (23)$$

According to Eq. (22), β_u vanishes at the fixed point.

As t vanishes, both numerator and denominator of the left-hand side of Eq. (13) go to zero if $\alpha < 0$, but the ratio has the universal value

$$\lim_{t \rightarrow 0} \left[\frac{R_0(t) - 1}{\alpha_{\text{eff}}^+(t)} \right] = \frac{1}{\alpha} \left[2^\alpha \frac{A'_0}{A_0} - 1 \right]. \quad (24)$$

It follows that Eq. (13) yields a value of u^* which depends only upon universal quantities and thus is independent of the pressure.¹¹ The value is (see also Ref. 11)

$$u^* = 0.0342. \quad (25)$$

We now have all the information needed to invert Eq. (13) and thereby to obtain $u(t)$ for $t \leq 10^{-2}$. For larger t , the specific heat is not known as well and is strongly influenced by regular transients which are not included in the theory. However, for $t > 10^{-2}$ the influence of u on the dynamics is quite small and thus $u(t)$ need not be known with high accuracy. In that temperature range we obtained $u(t)$ from an integration of

$$du(l)/dl = -\beta_u(l), \quad (26)$$

using Eq. (22) and starting with the small- t estimate, based on C_P and Eq. (13), as an initial value at $t = 10^{-2}$. Results for $u(t)/u^*$ at two pressures are given in Fig. 1. It can be seen that $u(t)$ calculated as described above evolves smoothly from u^* to zero as t grows from 0 to ∞ . In particular, the matching of the result based on Eq. (26) to that given by Eq. (13), which occurs at the value of

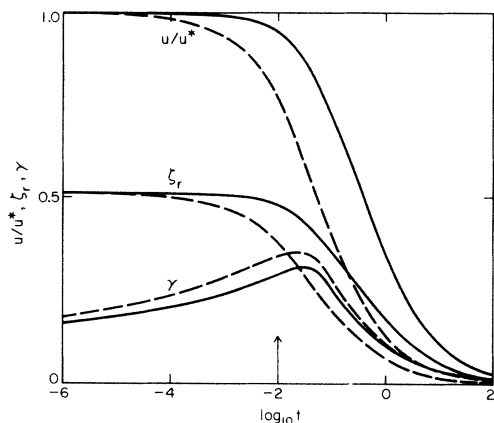


FIG. 1. Static coupling constants $u(t)$ derived from Eqs. (13) and (22) and $\gamma(t)$ [Eq. (27)], and the parameter $\zeta_r(t)$ [Eq. (19)], as a function of $\log_{10} t$. The solid lines pertain to vapor pressure and the dashed lines are for 28 bars. The arrow indicates the reduced temperature at which $u(t)$ obtained by integrating the beta-function equation (22) to higher t was matched onto the small- t result Eq. (13).

t indicated by the arrow, is quite smooth. In Fig. 1 we also illustrate the behavior of $\zeta_r(t)$ [Eq. (19)] which was obtained in the process of calculating $u(t)$. Since the calculation of $u(t)$ by the above procedure is somewhat complicated, we quote values below in Table III together with the dynamic parameters [once $u(t)$ is known, $\zeta_r(t)$ is easy to obtain from Eqs. (19), (20), and (25)].

The static coupling constant $\gamma[l(t)]$ which occurs in Eqs. (8) and (11) is given by Eq. (6.8) of Ref. 3, i.e.,

$$\gamma^2(t) = \frac{(2 - \zeta_r) \alpha_{\text{eff}}^+}{2\{2 + [2\zeta_r - 1 + (2 - \zeta_r) \alpha_{\text{eff}}^+](1 + 8u) + 8\beta_u\}} \quad (27)$$

with ζ_r , β_u , and u given by Eqs. (19)–(23), and the inversion of Eq. (13), respectively (for values of u , see also Table III).

For small t the effective specific-heat exponent α_{eff}^+ which is needed in Eq. (27) can be obtained directly from its definition, Eqs. (15) and (3). However, for large t , Eq. (3) for C_p has a minimum. This is illustrated by Fig. 2, where both data and C_p as given by Eq. (3) are shown at two illustrative pressures over a wide range of t . Beyond the minimum, where C_p increases with increasing t , α_{eff}^+ as given by Eq. (15) is negative. We presume that this effect is caused by the regular terms that contribute to C_p , and that it should not be included in the evaluation of the theory (which does not consider regular transients). In order to overcome this problem, we have adopted the previously proposed⁶ empirical formula

$$\alpha_{\text{eff}}^+ = \alpha_1/t + \alpha_2/t^2 \quad (28a)$$

for large t . This dependence upon t causes α_{eff}^+ to vanish smoothly in the large- t limit. The coefficients α_1 and α_2 were obtained by matching α_{eff}^+ and $d\alpha_{\text{eff}}^+/dt$ to the small- t results given by Eqs. (15) and (3) at a temperature t_m chosen so that $\alpha_{\text{eff}}^+(t_m) \cong 0.2$. The results of this composite procedure are shown in Fig. 3 for two pressures.

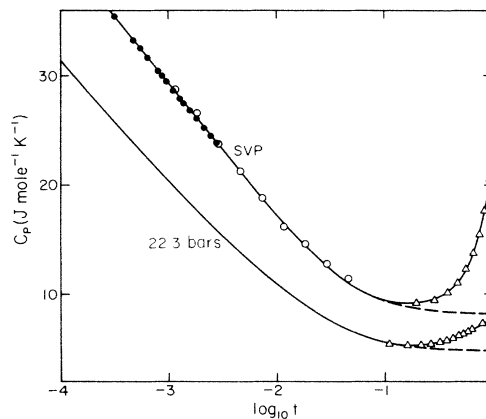


FIG. 2. Heat capacity at constant pressure C_p as a function of $\log_{10} t$ over a wide range of t . The various points are experimental data discussed in I. The dashed high-temperature extrapolations are our estimate of C_p in the absence of regular temperature dependences. They correspond to Eq. (28b) with the parameters in Table I.

Integrating Eq. (28a) gives our empirical estimate of the high-temperature singular specific heat in the form

$$C_p = C_{p,\infty} \exp(\alpha_1/t + \alpha_2/2t^2) \quad (28b)$$

We obtain $C_{p,\infty}$ by matching to C_p given by Eq. (3) at $t = t_m$. The parameters α_1 , α_2 , and $C_{p,\infty}$ for our isobars are given in Table I. The heat capacity given by Eq. (28) is shown as dashed lines in Fig. 2, and can be seen to be a smooth monotonic extrapolation of C_p at small t to $t > t_m$.

At this point we have all the information necessary to compute $\gamma(t)$. The results at two pressures are shown in Fig. 1 together with ζ_r and u/u^* . This completes the information necessary to (a) integrate the flow equations (11), starting, say, at $t_0 = 10^{-2}$ with initial values w'_0 , w''_0 , and F_0 given, and to (b) calculate $\hat{R}_\lambda(t)$ from the resulting $w'(t)$, $w''(t)$, and $F(t)$ using Eq. (8). Our procedure will

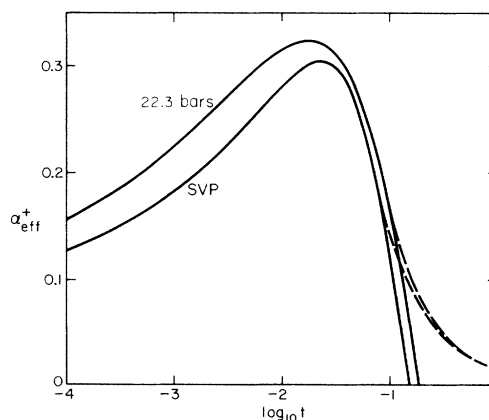


FIG. 3. Effective specific-heat exponent $\alpha_{\text{eff}}^+ = -d \ln C_p / d \ln t$ as a function of $\log_{10} t$. At small t , α_{eff}^+ is based on Eq. (3a). Those results become negative near $t = 10^{-1}$ (as shown by the solid lines) because regular transients cause C_p to have a minimum. Therefore, at large t , the dashed lines represent the empirical extrapolation via Eq. (28a).

TABLE I. Parameters for C_P and α_{eff} as given by Eq. (28) for $t > t_m$.

Pressure (bars)	t_m	$10^2\alpha_1$	$10^4\alpha_2$	$C_{P\infty}$ (J mole $^{-1}$ K $^{-1}$)
SVP	0.071	1.451	-0.284	8.121
6.85	0.075	1.922	-3.089	6.535
14.73	0.071	1.697	-2.124	5.527
22.30	0.084	1.529	1.076	4.812
28.00	0.063	1.344	-0.518	4.387

be to carry out this integration repeatedly, each time adjusting the initial values until a fit to the data is obtained.

The equations of model F given above simplify considerably when $\gamma = w'' = 0$. This simplification yields the two-loop flow equations for the symmetric planar spin model, model E of Halperin *et al.*¹ As discussed in the Introduction, for $|t| > 0$ model E is not expected to give an exact description of the contributions of thermal diffusion and second sound to the dynamics of the superfluid transition, but it provides a semiquantitative approximation. We will see below in Sec. III B to what extent model E can be used to fit the data. There we will actually use model E_s,⁶ which retains the heat capacity in the definition (2) of $\hat{R}_\lambda(t)$ but omits its coupling to the dynamic variables in the flow equations and in Eq. (8) for \hat{R}_λ .

C. Fixed point in two-loop order

The fixed-point values w^* and F^* of Eqs. (11) are obtained by setting $\beta_F(w, F, u, \gamma)$ and $\beta_w(w, f, u, \gamma)$ equal to zero, using $u = u^*$ as given by Eq. (25), setting $\gamma = 0$, and solving for w and F . We find

$$(w')^* = 0.0421, \quad (29a)$$

$$(w'')^* = 0.0000, \quad (29b)$$

$$F^* = 0.1866, \quad (29c)$$

and

$$f^* = 0.8256, \quad (29d)$$

where in the last equation we used Eq. (10). With Eq. (8) we then obtain the fixed-point value

$$R_\lambda = 1.074 \quad (29e)$$

of \hat{R}_λ . In order to see how important the two-loop contribution to R_λ is, we set M_3 equal to zero. This yielded $R_\lambda = 1.200$. Thus, at the fixed point the two-loop terms in \hat{R}_λ contribute only about 10%, as already estimated⁴ by Dohm.

Our results in Eq. (29) differ somewhat from those of Halperin *et al.*²¹ who used two-loop model-E flow equations. The fixed points of models E and F should be identical. We traced the difference to a somewhat different value of u^* in their calculations. They had²² $u^* = 0.1$, which gave $(w')^* = 0.018$, for instance. When we used our u^* [Eq. (25)] with their model-E flow equations, we obtained the results (29a)–(29d).

D. Method of analysis

The comparison between the experimental results and the theoretical predictions was carried out with a non-linear least-squares fitting procedure in which the initial values w_0 and $F_0(f_0, w_0)$ at some temperature t_0 were adjustable parameters. This was done by fitting the theoretical value $\hat{R}_\lambda^{\text{theor}}$ obtained from Eq. (8) to the experimental results $\hat{R}_\lambda^{\text{expt}}$ obtained from Eq. (2). The parameter t_0 was chosen to be $t_0 = 0.01$ and only data at reduced temperatures smaller than t_0 were used in the fits in order to avoid large uncertainties due to regular transients at large t . The procedure involved the following steps:

(i) The flow equations were integrated numerically with the chosen initial values of w'_0 , w''_0 , and F_0 using a fourth-order Runge-Kutta method²³ for ordinary differential equations. Since Eq. (11b) is complex, complex arithmetic had to be used.

(ii) The deviations between the experimental $\hat{R}_\lambda^{\text{expt}}$ and the theoretical $\hat{R}_\lambda^{\text{theor}}$ were then evaluated.

(iii) The initial values were adjusted so as to minimize the squared deviations given by the variance

$$\sigma^2 = \left[\left(\frac{N}{N-K} \right) \sum_{i=1}^N (\hat{R}_{\lambda,i}^{\text{expt}} - \hat{R}_{\lambda,i}^{\text{theor}})^2 W_i / \sum_{i=1}^N W_i \right], \quad (30)$$

where W_i is the weight attached to point i , N is the number of data points, and K is the number of adjustable parameters (for model F, $K=3$).

The weight for each data point was taken to be the inverse square of the probable error, i.e., $W = 1/(\delta\hat{R}_\lambda)^2$, where $\delta\hat{R}_\lambda$ is the *a priori* estimate of the probable error of $\hat{R}_\lambda^{\text{expt}}$. We have $\delta\lambda/\lambda = \delta\hat{R}_\lambda/\hat{R}_\lambda$, where $\delta\lambda$ is the probable error of λ . Thus

$$W = (\lambda^2/\hat{R}_\lambda^2)/(\delta\lambda)^2. \quad (31)$$

In general, the precision of the data was about 0.1%, except for small t , where temperature resolution ($\approx 5 \times 10^{-7}$ K) limited the precision of the data.⁵ Hence the probable error of λ was defined to be

$$\delta\lambda/\lambda = \max(10^{-3}, 5 \times 10^{-7}/\Delta T),$$

where δT was the temperature difference employed in each measurement (ΔT is given in Tables V–VII of I for this purpose).

The fits yielded the best values of the adjusted parameters, the probable errors in these quantities, and the deviation σ from the fit. By suitable choice of initial conditions, the fits converged in 6 to 20 iterations. Nonetheless, it would have been very computer-time consuming if the complete set of experimental data for each isobar had been used. Thus, only about ten data points per decade, as given in Table VI of I for cell F, were used in the fits.

All the calculations were performed on a Digital Equipment Corporation VAX11/750 computer in FORTRAN, using complex arithmetic. Typically, six iterations with 35 data points required 30 min of CPU (central processing unit) time.

TABLE II. Parameters derived from fits of the two-loop model-F theory with static transients to data with $t \leq t_0 = 10^{-2}$. The lower limit of the reduced temperature ranges over which data were used is t_{\min} , and $f_0 = f(t_0)$, $w'_0 = w'(t_0)$, $w''_0 = w''(t_0)$. The standard deviation from the fit is σ [Eq. (30)], and N is the number of points used in the fit. The parameters in the first five rows are our standard fits.

	Cell	P (bars)	$\log_{10} t_{\min}$	f_0	w'_0	w''_0	$10^3 \sigma$	N
1	<i>F</i>	SVP	-6	0.612(2)	0.644(2)	1.398(19)	1.01	36
2	<i>F</i>	6.85	-6	0.424(2)	0.722(2)	1.219(24)	1.10	32
3	<i>F</i>	14.73	-6	0.289(3)	0.795(5)	1.072(50)	2.00	36
4	<i>F</i>	22.30	-6	0.205(1)	0.899(4)	0.919(38)	1.18	36
5	<i>F</i>	28.00	-6	0.155(1)	0.919(4)	0.552(29)	0.81	36
6	<i>F</i>	6.85	-2.6	0.430(3)	0.713(3)	0.939(169)	0.11	5
7	<i>F</i>	14.73	-2.8	0.298(7)	0.771(28)	0.891(145)	0.29	9
8	<i>F</i>	22.30	-3.1	0.206(2)	0.900(9)	0.263(146)	0.58	11
9	<i>F</i>	28.00	-3.3	0.158(1)	0.911(5)	0.368(110)	0.46	13
10	<i>E</i>	SVP	-6	0.597(7)	0.662(3)	1.340(31)	1.23	33
11	<i>E</i>	22.30	-6	0.208(9)	0.897(9)	0.626(54)	1.45	26

E. Numerical tests

It is apparent from Secs. IIB and IID that the numerical procedure is quite complicated. Thus a number of tests of our computer code were performed in order to check its reliability. A partial test of our flow equations is given by finding the roots which gave the fixed-point values (29a)–(29d). As mentioned above, the results agree with those obtained from the much simpler model-E flow equations. In addition, $(w'')^*$ is known to be equal to zero. We found typically $|(w'')^*| = O(10^{-11})$ from our numerical procedure.

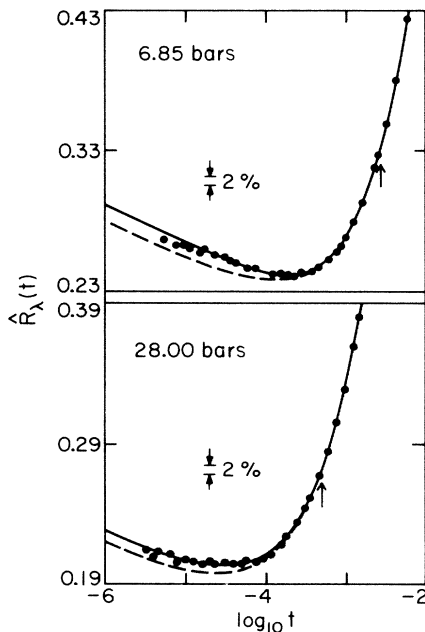


FIG. 4. Fits to the data of the complete two-loop model-F theory with static transients. The solid lines represent fits using data over the entire range $t \leq t_0 = 10^{-2}$. They are our standard fits. Standard fits to the data at other pressures can be seen in Fig. 8 below. The dashed lines represent extrapolations to small t of limited-range fits, using data only for t larger than the value indicated by the arrows (and smaller than $t_0 = 10^{-2}$). For the data used in the limited-range fits, we have $f \leq 0.8$.

As a test of our integration procedure, we integrated the complete flow equations with $u(t)$ and $\gamma(t)$ and with typical initial values from $t_0 = 10^{-2}$ to $t_{\min} = 10^{-50}$ and $t_{\min} = 10^{-100}$, and obtained

$$\begin{aligned} w'(t_{\min}) &= 0.05857, 0.04473, \\ w''(t_{\min}) &= 0.00078, 0.00021, \\ F(t_{\min}) &= 0.2210, 0.1923, \end{aligned} \quad (32)$$

where the first value corresponds to $t_{\min} = 10^{-50}$. These results still differ from the fixed-point values; but the differences are still decreasing as t decreases and illustrate the slowness of the dynamic transients. The results are close enough to the fixed-point values to convince us of the reliability of our numerical procedure.

There are a number of analytic results which may be

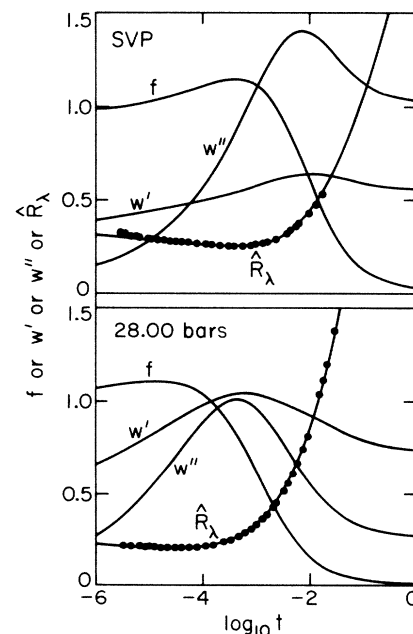


FIG. 5. Functions $f(t)$, $w'(t)$, $w''(t)$, and $\hat{R}_\lambda(t)$ over a wide range as a function of $\log_{10} t$ obtained from our standard fits.

TABLE III. (Continued).

$\log_{10}t$	u	w'	f	w''	$\log_{10}t$	u	w'	f	w''
$P=22.30$ bars					$P=28.00$ bars				
-5.2	0.0341	0.6482	1.0879	0.4172	-6.4	0.0342	0.6078	1.0518	0.2082
-5.0	0.0340	0.6741	1.0978	0.4774	-6.2	0.0342	0.6331	1.0597	0.2390
-4.8	0.0340	0.7011	1.1065	0.5454	-6.0	0.0342	0.6598	1.0677	0.2740
-4.6	0.0339	0.7294	1.1126	0.6215	-5.8	0.0342	0.6878	1.0757	0.3138
-4.4	0.0339	0.7587	1.1142	0.7053	-5.6	0.0342	0.7172	1.0835	0.3587
-4.2	0.0338	0.7888	1.1087	0.7955	-5.4	0.0341	0.7479	1.0907	0.4092
-4.0	0.0337	0.8195	1.0925	0.8895	-5.2	0.0341	0.7797	1.0969	0.4655
-3.8	0.0335	0.8499	1.0616	0.9827	-5.0	0.0340	0.8126	1.1012	0.5276
-3.6	0.0334	0.8788	1.0121	1.0687	-4.8	0.0340	0.8462	1.1023	0.5953
-3.4	0.0331	0.9045	0.9410	1.1391	-4.6	0.0339	0.8802	1.0988	0.6675
-3.2	0.0329	0.9250	0.8480	1.1854	-4.4	0.0338	0.9139	1.0884	0.7425
-3.0	0.0325	0.9385	0.7369	1.2011	-4.2	0.0337	0.9464	1.0682	0.8173
-2.8	0.0321	0.9439	0.6153	1.1843	-4.0	0.0335	0.9765	1.0351	0.8874
-2.6	0.0315	0.9413	0.4932	1.1386	-3.8	0.0333	1.0027	0.9860	0.9470
-2.4	0.0308	0.9319	0.3803	1.0724	-3.6	0.0331	1.0230	0.9186	0.9892
-2.2	0.0298	0.9173	0.2833	0.9959	-3.4	0.0328	1.0357	0.8324	1.0075
-2.0	0.0286	0.8992	0.2051	0.9188	-3.2	0.0324	1.0393	0.7299	0.9975
-1.6	0.0247	0.8568	0.1019	0.7891	-3.0	0.0319	1.0337	0.6167	0.9582
-1.2	0.0201	0.8093	0.0500	0.7047	-2.8	0.0312	1.1095	0.5013	0.8938
-0.8	0.0157	0.7650	0.0269	0.6506	-2.6	0.0304	0.9988	0.3921	0.8120
-0.4	0.0119	0.7394	0.0161	0.6199	-2.4	0.0294	0.9738	0.2961	0.7223
0.0	0.0089	0.7284	0.0103	0.6056	-2.2	0.0280	0.9467	0.2170	0.6336
1.0	0.0046	0.7228	0.0044	0.5965	-2.0	0.0263	0.9191	0.1553	0.5524
2.0	0.0027	0.7226	0.0024	0.5958	-1.6	0.0219	0.8647	0.0770	0.4258
3.0	0.0018	0.7227	0.0015	0.5959	-1.2	0.0174	0.8118	0.0392	0.3461
					-0.8	0.0133	0.7696	0.0223	0.3019
					-0.4	0.0101	0.7467	0.0140	0.2803
					0.0	0.0077	0.7369	0.0094	0.2705
					1.0	0.0042	0.7317	0.0044	0.2641
					2.0	0.0026	0.7313	0.0026	0.2633
					3.0	0.0017	0.7313	0.0016	0.2633
$P=28.00$ bars									
-7.0	0.0343	0.5397	1.0298	0.1373					
-6.8	0.0342	0.5611	1.0369	0.1578					
-6.6	0.0342	0.5838	1.0442	0.1813					

compared with the numerical work. Perhaps foremost among these is the invariance of the model-F Langevin equations under a simultaneous change of the sign of F and w'' [leaving the signs of γ , u , and w' (which are intrinsically positive) unaltered].⁴ Indeed, we obtained the same fit to a given set of data with positive and negative F_0 and w''_0 , in the sense that w' , $|F|$, $|w''|$, and σ (the square root of the variance) were the same within a few parts in 10^4 .

We have also reproduced with our computer code the analytic results (4.18), (4.19), and (A35)–(A38) of Ref. 4. Finally, we compared the integration of the two-loop model-F flow equations (with $u=u^*$) with a numerical example kindly provided by Folk. Our results agreed with his.

III. RESULTS

A. Two-loop model-F fits with static transients

Our main results are the fits of the two-loop model-F flow equations (11) and the two-loop expression (8) for \hat{R}_λ , including the static transients contained in $u(t)$ and $\gamma[u(t)]$, to the experimental values of $\hat{R}_\lambda(t)$ for cell F of

I. As mentioned earlier, all of the fits are for $t \leq t_0 = 10^{-2}$. Parameters for fits to all data with $t \leq t_0$ are given in rows 1–5 of Table II. Also given in that table is the standard deviation σ defined by Eq. (30) and the number of data points, N , involved in the fit. Since \hat{R}_λ is typically close to 0.3 in the experimental range, the values of σ are about 0.2% or 0.3% of \hat{R}_λ and thus of the same size as the random experimental errors (see I). In Fig. 4 we show the data at 6.85 bars and at 28.00 bars, together with the corresponding fits (solid lines). Here, also, one sees that the data deviate more or less randomly from the solid lines. The results at the other pressures may be seen in Fig. 8 below.

Having obtained a statistically meaningful fit of the theory to the data, it is of interest to examine the corresponding behavior of the dynamic variables in the theory. In Fig. 5 we show f , w' , w'' , and \hat{R}_λ over the wide range $10^{-6} \leq t \leq 1$ and for the two extreme pressures SVP and 28 bars. Even at the smallest reduced temperature w' and \hat{R}_λ are still far away from their fixed-point values. The imaginary part w'' of w seems to approach its value $(w'')^* = 0$ somewhat more rapidly.

Particularly relevant to our analysis is the behavior of f

TABLE IV. High-temperature values of the dynamic parameters obtained by integrating the flow equations from $t_0 = 10^{-2}$ to $t = 10^3$, with parameters taken from rows 1–5 and 10–11 of Table II. The last column gives $\Gamma_\infty'' = w_\infty'' \lambda_{\infty 0} / C_{P_\infty}$, with $\lambda_{\infty 0}$ from Table IX of I and C_{P_∞} from Table I.

Cell	P (bars)	w_∞'	w_∞''	$10^4 \Gamma_\infty''$ (cm ² /sec)
F	SVP	0.559	1.029	4.48
F	6.84	0.571	0.817	4.41
F	14.73	0.625	0.705	4.48
F	22.30	0.723	0.596	4.22
F	28.00	0.731	0.263	1.96
E	SVP	0.570	0.970	4.22
E	22.30	0.694	0.289	2.05

at large t . We see that $f = O(1)$ for $t \lesssim 5 \times 10^{-3}$ at SVP and for $t \lesssim 5 \times 10^{-4}$ at 28.00 bars. Thus, the fits given by the first five rows in Table II involved two to three decades (depending upon P) over which a low-order perturbation calculation of the flow equations and of $\hat{R}_\lambda(f, w, u, \gamma)$ is not necessarily reliable (because the expansion parameter f of the theory is not small compared to unity). We therefore repeated the fits, but restricted the range of the data to values of t for which $f \leq 0.8$ (we retained 10^{-2} as the upper limit). At vapor pressure this restriction was too severe, leaving only one-third of a decade and rather few data points. For 6.86 bars, the fit included half a decade, and extended from the small vertical arrow in Fig. 4 to the right-hand edge of that figure. At 28.00 bars the available range of t spanned 1.3 decades as indi-

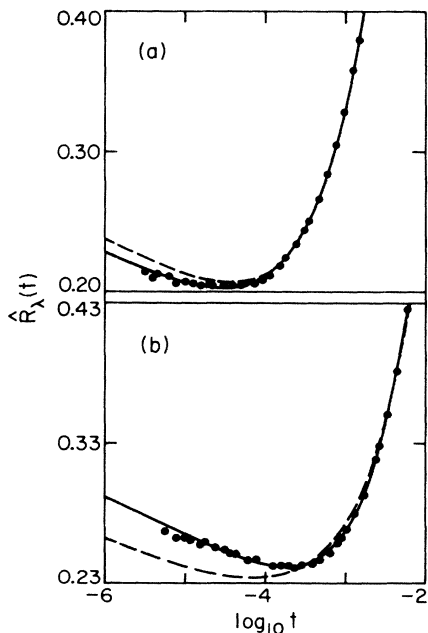


FIG. 6. Fit of the two-loop model-F theory over the range $t \leq t_0 = 10^{-2}$ to the data of $\hat{R}_\lambda(t)$. The solid lines are the standard fits. The dashed lines correspond to w_0'' held fixed. (a) $P = 28$ bars, $w_0'' = 0.8$. This corresponds to $\Gamma_\infty'' = 4 \times 10^{-4}$ cm²/sec. (b) $P = 6.8$ bars, $w_0'' = 0.5$. This corresponds to $\Gamma_\infty'' = 0.8 \times 10^{-4}$ cm²/sec.

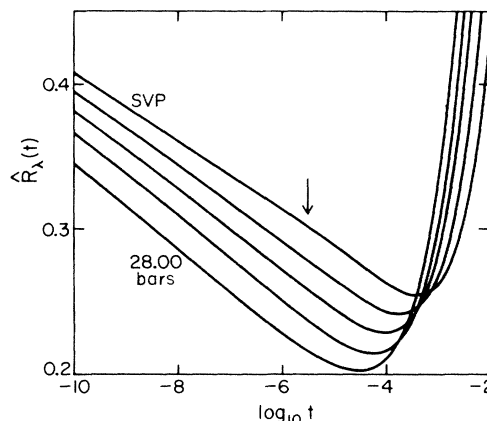


FIG. 7. Results for \hat{R}_λ based on the standard fits and for all pressures over a wide range of t , as a function of $\log_{10} t$. Near the left-hand margin, the lines correspond, from top to bottom, to SVP, 6.85, 14.73, 22.30, and 28.00 bars. The arrow indicates the smallest value of t at which data exist.

cated by the arrow in the lower portion of Fig. 4. The results of the limited-range fits are given in rows 6–9 of Table II. As can be seen, the parameter values are not very different from those obtained by the full-range fits

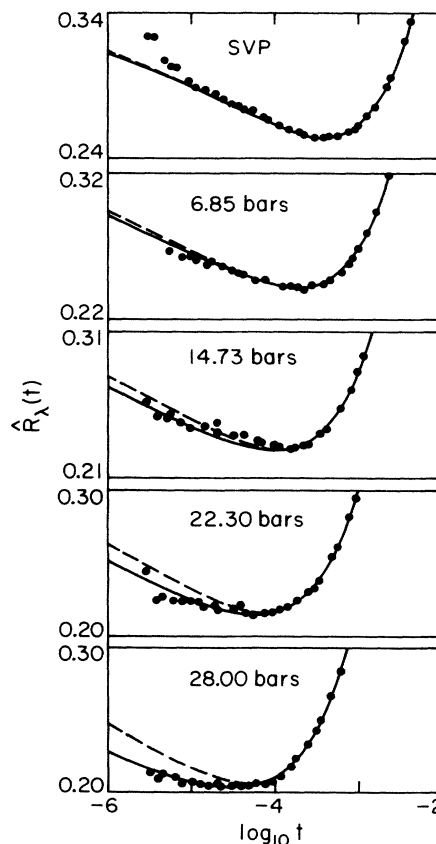


FIG. 8. Fits of the two-loop model-F theory with $u = u(t)$ (standard fit, solid lines) and with $u = u^*$ (dashed lines) to the data for $\hat{R}_\lambda(t)$ on each experimental isobar. At low P , the t dependence of u has a negligible influence; but at the higher pressures a good fit cannot be obtained when the t dependence of u is neglected.

TABLE V. Parameters obtained by fitting incomplete theoretical expressions for \hat{R}_λ and/or the flow equations to cell-F data with $t \leq t_0 = 10^{-2}$. Rows 1–5: $u = u^*$ in \hat{R}_λ and in the flow equations. Rows 6–10: \hat{R}_λ [Eq. (8)] to one-loop order, but two-loop flow equations. Rows 11–15: $\gamma = w'' = 0$ (model E) in \hat{R}_λ only. Rows 16–20: $\gamma = w'' = 0$ in \hat{R}_λ and in the flow equations. As in Table II, $f_0 = f(t_0)$, $w'_0 = w'(t_0)$, and $w''_0 = w''(t_0)$.

	P (bars)	f_0	w'_0	w''_0	$10^3\sigma$	N
1	SVP	0.601(2)	0.656(1)	1.435(16)	0.85	36
2	6.85	0.412(2)	0.744(2)	1.313(18)	0.81	32
3	14.73	0.274(2)	0.835(4)	1.307(36)	1.43	36
4	22.30	0.191(1)	0.968(4)	1.342(43)	1.28	36
5	28.00	0.137(2)	1.046(13)	1.279(108)	2.79	36
6	SVP	0.525(2)	0.737(1)	1.131(13)	0.70	36
7	6.85	0.361(2)	0.821(2)	0.955(21)	0.99	32
8	14.73	0.243(2)	0.898(5)	0.829(44)	1.75	36
9	22.30	0.174(1)	1.004(5)	0.661(35)	1.12	36
10	28.00	0.133(1)	1.008(6)	0.300(25)	0.77	36
11	SVP	0.619(3)	0.451(1)	0.982(8)	0.78	36
12	6.85	0.445(2)	0.515(1)	0.926(8)	0.67	32
13	14.73	0.302(3)	0.560(4)	0.943(16)	1.16	36
14	22.30	0.214(2)	0.640(5)	0.924(22)	1.18	36
15	28.00	0.152(3)	0.681(11)	0.809(40)	1.78	36
16	SVP	0.439(10)	0.895(11)		5.78	36
17	6.85	0.285(14)	1.085(34)		10.68	32
18	14.73	0.158(15)	1.495(107)		15.69	36
19	22.30	0.099(13)	1.972(200)		17.91	36
20	28.00	0.039(13)	3.945(1.205)		24.06	36

(rows 1–5 of Table II). An extrapolation of the limited-range fits to small t is shown in Fig. 4 as dashed lines for the two representative pressures (the results at 14.73 and 22.30 bars behave in a similar manner). It is truly remarkable that the theory, when extrapolated by *two* (at 28 bars) or *three* (at 6.85 bars) decades, differs from the data by only 2% or 3%. These limited-range fits provide the justification for the full-range fits (rows 1–5 in Table II), which include data at temperatures where the dynamic coupling constant is of order one. Of course, the reason for the unexpectedly spectacular success of the theory is

not obvious.

We retained the full-range fits as our standard fits, and used them to generate values of f , w' , and w'' over a wide range of t . These data, together with values of $u(t)$, are given in Table III. They may be used in the prediction of other transport properties, including the damping of second sound and the dynamic structure factor.

In I we presented independent sets of measurements at vapor pressure and 22.3 bars for a cell of spacing $d=0.452$ cm (cell E). These data were not quite as accurate as the cell-F data, and there were small but systemat-

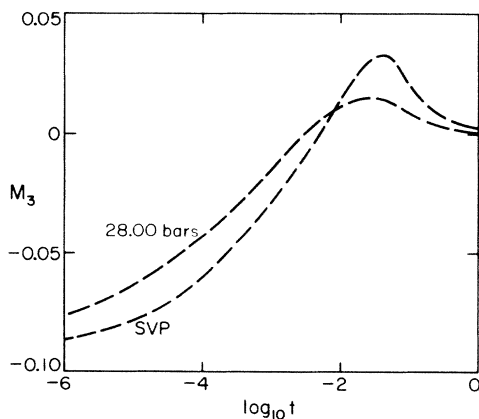


FIG. 9. Two-loop contribution M_3 to \hat{R}_λ as a function of $\log_{10} t$.

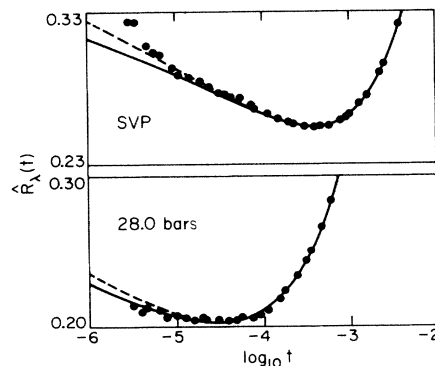


FIG. 10. Effect of neglecting the two-loop contributions to \hat{R}_λ upon a fit of model F (two-loop flow equations with static transients) to the data. Solid lines: standard fit. Dashed lines: one-loop \hat{R}_λ .

ic differences between the data sets at the same pressure.⁵ The parameters for the full-range fits ($t < 10^{-2}$) to the cell-E data are given in rows 10 and 11 of Table II. Any differences from the corresponding parameter values for cell F (rows 1 and 4 in Table II) are indicative of the influence of possible systematic errors in the data (although we regard the cell-F data as more accurate). Generally, the parameters are quite similar for the two cells, but w_0'' at the higher pressure differs considerably. It turns out that w_0'' is particularly sensitive to small systematic changes in the data.

It has been suggested by Dohm²⁴ that the parameter

$$\Gamma_\infty'' = w_\infty'' \lambda_{\infty 0} / C_{P_\infty} \quad (33)$$

should be pressure independent and approximately equal to $\hbar/2m_4 = 0.79 \times 10^{-4}$ cm²/sec. Here w_∞'' is the high-temperature value of w'' , and $\lambda_{\infty 0}$ and C_{P_∞} are the high-temperature extrapolations of λ and C_P . We integrated the flow equations with the initial values given in rows 1–5 and 10 and 11 of Table II out to $t = 10^3$. Note that for this purpose we had to use the empirical extrapolation (28) of the specific heat, and values of $u(t)$ obtained by integrating Eq. (26). Beyond $t = 1$, w' and w'' changed very little, as can be seen also from Table III. We give the high-temperature limits of w' and w'' in Table IV. Using values of $\lambda_{\infty 0}$ from Table IX of I and C_{P_∞} from Table I, we obtained the results for Γ_∞'' given in the last column of Table IV. For cell F and $P < 22.3$ bars, this parameter is remarkably constant, as predicted, but at the highest pressure it suddenly changes by a factor of 2. However, at 22.30 bars the cell-E result is lower than the cell-F value by about a factor of 2, and thus the variation Γ_∞'' with pressure is probably within its systematic uncertainty. The value of Γ_∞'' is larger than predicted by a factor of $2\frac{1}{2}$ –5.

In order to explore further whether the experimental data at 28 bars are inconsistent with the low-pressure result $\Gamma_\infty'' = 4 \times 10^{-4}$ cm²/sec, we fixed w_0'' (i.e., w'' at $t_0 = 10^{-2}$) at the value 0.8 and refitted the cell-F \hat{R}_λ data at 28 bars and for $t < t_0$, adjusting the other parameters, f_0 and w_0' . The fit and the value chosen for w_0'' , upon integration to high t , yield $\Gamma_\infty'' = 4 \times 10^{-4}$ cm²/sec. In Fig. 6(a) we show the result as a dashed line. The solid line is the standard, unconstrained fit which yielded $\Gamma_\infty'' = 2 \times 10^4$ cm²/sec. The deviations of the constrained fit from the data, although not large, are systematic.

In Fig. 6(b) we show the result of the procedure described in the preceding paragraph, but for $P = 6.85$ bars and cell F and with w_0'' fixed at 0.5. The corresponding fit, when integrated to high t , yields the estimate²⁴ $\Gamma_\infty'' = 0.8 \times 10^{-4}$ cm²/sec. Clearly, this constraint is inconsistent with the experimental data. Thus we conclude that Γ_∞'' is significantly larger than the estimate of Ref. 24.

We conclude this section by presenting in Fig. 7 an extrapolation of $\hat{R}_\lambda(t)$, based on the full-range fits, to smaller values of t . At present, experimental data exist to the right of the small arrow in the figure. To the left of the arrow, $\hat{R}_\lambda(t)$ is still far away from its fixed-point value 1.074 and increasing significantly. Eventually, it might be

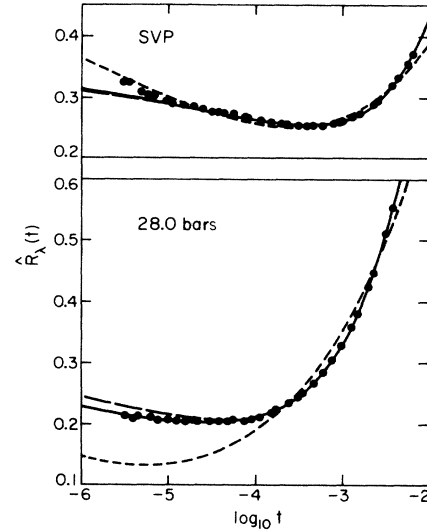


FIG. 11. Effect of using a two-loop model-E_s theory rather than model F. The solid lines represent the standard model-F fits. The long-dashed lines are the result of a fit in with $\gamma = w'' = 0$ in the formula for \hat{R}_λ (but not in the flow equations). The short-dashed lines are a fit of the complete two-loop model E_s, with $\gamma = w'' = 0$ in the flow equations as well as in \hat{R}_λ .

possible to obtain experimental data over perhaps two additional decades and thereby provide a further test of the theoretical predictions.

B. Other fits

Although the preceding subsection contains the main results of our work, it is of interest to see how well the theory fits the data when certain terms are neglected or

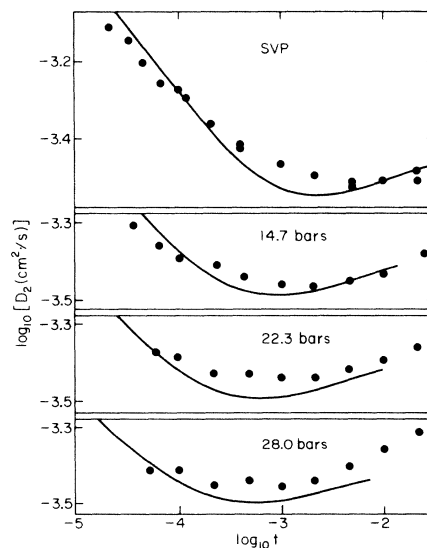


FIG. 12. Second-sound damping D_2 as a function of the reduced temperature t on logarithmic scales at the four indicated pressures. The data points are from Ref. 26. The solid lines are calculated from u , f , and w' in Table III, and from the model-E formulas of Ref. 25 with $\xi_L/\xi_T = 0.37$.

certain approximations are made. These fits to incomplete or approximate theoretical predictions are presented in this section.

In Fig. 8 we show as dashed lines the fits which result from setting $u(t)$ equal to its fixed-point value u^* . The solid lines are the standard fits. This approximation also changes ζ_r to the value given by Eq. (21) and slightly alters $\gamma(t)$ [Eq. (27)]. The static transients in Eq. (2), which come from Eqs. (3a) and (5), are retained, however, so that the data for $\hat{R}_\lambda(t)$ remain unaltered. It is apparent from Fig. 8 that the static transients presented by the t dependence of u are unimportant at vapor pressure, but their neglect at the higher pressures clearly results in an imperfect fit of the theory to the data. The parameters resulting from the fit with $u(t)=u^*$ are given in the first five rows of Table V.

Next we investigated the importance of the two-loop contribution to $\hat{R}_\lambda(f, w, \gamma, u)$, Eq. (8). In Fig. 9 we plot the term M_3 which results from our standard fits at SVP and at 28 bars. We find that M_3 is quite small for $t \geq 5 \times 10^{-4}$, and thus in that range the two-loop contribution fM_3 in Eq. (8) is negligible. Even for smaller t , where fM_3 potentially could have been important because f has grown to be of $O(1)$, M_3 itself remains of modest magnitude and fM_3 contributes only about 10% or less to \hat{R}_λ . It is interesting to note that the value of w'' is determined in the fits primarily through its contribution to M_3 (it also occurs in the flow equations, but there it couples only indirectly through the other dynamic variables to the experimental data). An accurate determination of w'' therefore can be hoped for only when data for $t \leq 5 \times 10^{-4}$ are included in the fit.

In Fig. 10 we illustrate the effect on the fit to the data of neglecting the two-loop contribution to \hat{R}_λ by setting $M_3=0$ and omitting the contribution $16\gamma^2 u$ to Eq. (8). The parameters obtained under these conditions (but retaining the full two-loop model-F flow equations with all static transients) are given in rows 6–10 of Table V. It is apparent that an essentially perfect fit to the data can be obtained with the one-loop result for \hat{R}_λ .

Finally, in Fig. 11 we show the effect of using the symmetric planar spin model,¹ model E_s,⁶ which neglects the coupling of the specific heat to the dynamics. First, as long-dashed lines we give the results of setting w'' and γ equal to zero only in Eq. (8) for \hat{R}_λ , retaining the full model-F flow equations. At vapor pressure this has very little influence on the quality of the fit, but at the higher

pressure the fit is not quite as good as the full model-F fit represented by the solid lines. The parameters for these fits are given in rows 11–15 of Table V. Lastly, as short dashed lines, we show the result of using a complete model-E_s theory. These fits were obtained by setting $w''=\gamma=0$ in the flow equations as well as in \hat{R}_λ . The fit is unsatisfactory even at vapor pressure. At the higher pressure it is very poor indeed. The corresponding parameters are given in rows 16–20 of Table V.

C. Second-sound damping

In principle, the second-sound damping below T_λ can be obtained from the values of f and w determined above T_λ without any further adjustable parameters. In practice, there remain two problems. First, the relation $D_2(f, w, u)$ has been obtained so far only for model E.²⁵ Therefore we do not necessarily expect perfect agreement of the theory with the data.²⁶ The second problem is associated with the necessary static parameters. The formula for D_2 involves not only $u(t)$ (which is known quite well now), but also the ratio ξ_L/ξ_T of the longitudinal to the transverse correlation length. This ratio is a universal constant, and from an expansion in $4-d$ it is estimated to be approximately $\frac{1}{3}$. We will treat it as an adjustable parameter, but the same value of ξ_L/ξ_T will be used at all pressures. For the best value we find 0.37, rather close to the $(4-d)$ -expansion value of the theory.

In Fig. 12 we compare the model-E prediction²⁵ $D_2(f, w', u)$, using the values of $f(t)$, $w'(t)$, and $u(t)$ in Table III and $\xi_L/\xi_T=0.37$, with the experimental results²⁶ for D_2 . The agreement is remarkably good, but there remain systematic differences between theory and experiment which persist at all pressures. We attribute these differences to the use of model E rather than model F in the calculation of $D_2(f, w', u)$.

ACKNOWLEDGMENTS

We appreciate the illuminating discussions which we had with P. C. Hohenberg throughout the course of this work. We are grateful to R. Folk for providing us with a numerical example of the flow-equation integration, and to V. Dohm for communicating his theoretical results to us as soon as they became available and prior to publication. This work was supported by National Science Foundation Grant No. DMR-84-14804.

¹B. I. Halperin, P. C. Hohenberg, and E. D. Siggia, Phys. Rev. Lett. **32**, 1289 (1974); Phys. Rev. B **13**, 1299 (1976); P. C. Hohenberg and B. I. Halperin, Rev. Mod. Phys. **49**, 435 (1977).

²V. Dohm (unpublished). A preliminary report is available from V. Dohm.

³V. Dohm, Z. Phys. B **60**, 61 (1985).

⁴V. Dohm, Z. Phys. B **61**, 193 (1985).

⁵W. Y. Tam and G. Ahlers, Phys. Rev. B **32**, 5932 (1985).

⁶G. Ahlers, P. C. Hohenberg, and A. Kornblit, Phys. Rev. Lett.

36, 493 (1981); Phys. Rev. B **25**, 3136 (1982).

⁷V. Dohm and R. Folk, Phys. Rev. Lett. **46**, 349 (1981); Z. Phys. B **40**, 79 (1980).

⁸For reviews of recent developments in this field, see V. Dohm and R. Folk, in *Advances in Solid State Physics*, edited by P. Grosse (Vieweg, Braunschweig, 1982), Vol. 22; V. Dohm and R. Folk, Physica **109&110B**, 1549 (1982); P. C. Hohenberg, *ibid.* **109&110B**, 1436 (1982); G. Ahlers, in *Phase Transitions*, edited by M. Levy, J. C. le Guillou, and J. Zinn-Justin (Plenum, New York, 1980), p. 1; G. Ahlers, Rev. Mod. Phys. **52**,

- 489 (1980). A recent extensive experimental investigation and the comparison of its results with the theory are reported by R. Mehrotra and G. Ahlers, *Phys. Rev. B* **30**, 5116 (1984).
- ⁹A different theoretical treatment of the dynamics of the superfluid transition has been given by R. A. Ferrell and J. K. Bhattacharjee, *Phys. Rev. Lett.* **42**, 1638 (1979); *J. Low Temp. Phys.* **36**, 165 (1979). Although these authors have not published the Langevin equations upon which their work is based, it appears to us that their model of the dynamics is less complete than model F of Ref. 1 and does not fully include the contributions of thermal diffusion and second sound. In addition, it is not clear to us that their calculations correspond to a systematic truncation of the theory. For the field-theoretic work (Refs. 2 and 4) on models E and F it is clear that the theory is complete to two-loop order in the coupling constants. For those reasons we consider in the *quantitative* comparison of *this* paper only the perturbation calculations by Dohm (Refs. 2 and 4) based on models E and F of Halperin, Hohenberg, and Siggia (Ref. 1).
- ¹⁰D. S. Greywall and G. Ahlers, *Phys. Rev. Lett.* **28**, 1251 (1972); *Phys. Rev. A* **7**, 2145 (1973); G. Ahlers, *ibid.* **3**, 696 (1971); K. H. Mueller, G. Ahlers, and F. Pobell, *Phys. Rev. B* **14**, 2096 (1976).
- ¹¹A. Singaas and G. Ahlers, *Phys. Rev. B* **29**, 4951 (1984); **30**, 5103 (1984).
- ¹²V. Dohm and R. Folk, *Z. Phys. B* **45**, 129 (1981).
- ¹³P. C. Hohenberg, B. I. Halperin, and D. R. Nelson, *Phys. Rev. B* **22**, 2373 (1980).
- ¹⁴K. G. Wilson, *Phys. Rev. B* **4**, 3174 (1971); **4**, 3184 (1971). See also K. G. Wilson and J. Kogut, *Phys. Lett.* **12C**, 76 (1974); M. E. Fisher, *Rev. Mod. Phys.* **46**, 597 (1974).
- ¹⁵W. Y. Tam, Ph.D. thesis, University of California, Santa Barbara, 1985. See AIP document no. PAPS (PRBMD-32-5932-62) for 62 pages of experimental data. Order by PAPS number and journal reference from American Institute of Physics, Physics Auxiliary Publication Service, 335 East 45th Street, New York, N.Y. 10017. The price is \$1.50 for a microfiche, or \$5.00 for a photocopy. Airmail additional. Make checks payable to the American Institute of Physics.
- ¹⁶The asymptotic power-law behavior was predicted already by the dynamic scaling theory (Ref. 17) which preceded the renormalization-group treatment of transport properties.
- ¹⁷R. A. Ferrell, N. Menyhard, H. Schmidt, F. Schwabl, and P. Szeffalussy, *Phys. Rev. Lett.* **18**, 891 (1967); *Phys. Lett.* **24A**, 493 (1967); *Ann. Phys. (N.Y.)* **47**, 565 (1968); B. I. Halperin and P. C. Hohenberg, *Phys. Rev. Lett.* **19**, 700 (1967); *Phys. Rev.* **177**, 952 (1969).
- ¹⁸C. Bagnuls and C. Bervillier, *Phys. Rev. B* **24**, 1226 (1981).
- ¹⁹A. Aharony and G. Ahlers, *Phys. Rev. Lett.* **44**, 782 (1980); M. C. Chang and A. Houghton, *Phys. Rev. B* **21**, 1881 (1980); *Phys. Rev. Lett.* **44**, 785 (1980).
- ²⁰These equations follow from Eqs. (3.15) and (3.16) of Ref. 4 if l is defined by Eq. (7a).
- ²¹P. C. Hohenberg, B. I. Halperin, and D. Nelson, *Phys. Rev. B* **22**, 2373 (1980).
- ²²The normalization of the coupling constant u used in Ref. 21 differs from that used by Dohm in Refs. 2–4 and in the present paper by a factor of $4!/4=6$. Thus, their value of $u^*=0.6$ corresponds to 0.1 in the normalization used by Dohm and here.
- ²³E. V. Krishnamurthy and S. K. Sen, *Computer-Based Numerical Algorithms* (Affiliated East-West, New Delhi, 1976).
- ²⁴V. Dohm, *Phys. Rev. B* **29**, 1497 (1984).
- ²⁵V. Dohm and R. Folk, *Phys. Rev. Lett.* **46**, 349 (1981); *Z. Phys. B* **41**, 251 (1981).
- ²⁶R. Mehrotra and G. Ahlers, *Phys. Rev. Lett.* **51**, 2116 (1983); *Phys. Rev. B* **30**, 5116 (1984).